applied sciences

MDPI

Article

Effect of Post-Annealing on the Microstructure and Microwave Dielectric Properties of $Ba(Co_{0.7}Zn_{0.3})_{1/3}Nb_{2/3}O_3$ Ceramics

Brahim Itaalit [1], Mohamed Mouyane [1,*], Jérôme Bernard [1], Manfred Womes [2] and David Houivet [1]

Received: 29 October 2015; Accepted: 3 December 2015; Published: 22 December 2015
Academic Editor: Sheng-Yuan Chu

[1] Laboratoire Universitaire des Sciences Appliquées de Cherbourg (LUSAC), Université de Caen Basse-Normandie (UCBN), EA 4253, Site Universitaire-60 rue Max Pol Fouchet, CS 20082, Cherbourg-Octeville 50130, France; brahim.itaalit@unicaen.fr (B.I.); jerome.bernard@unicaen.fr (J.B.); david.houivet@unicaen.fr (D.H.)

[2] Institut Charles Gerhardt, Equipe Agrégats, Interfaces et Matériaux pour l'Energie, Unité Mixte de Recherche (UMR 5253), Centre National de la Recherche Scientifique (CNRS), Université Montpellier II, Cedex 5, Montpellier 34095, France; manfred.womes@orange.fr

* Correspondence: mohamed.mouyane@unicaen.fr; Tel.: +33-1-0233-4549; Fax: +33-2-3301-4135

Abstract: The effects of post-annealing on the crystal structure, microstructure, and microwave dielectric properties for $Ba(Co_{0.7}Zn_{0.3})_{1/3}Nb_{2/3}O_3$ ceramics were investigated. The as-prepared materials were characterized by X-ray diffraction, scanning electron microscopy and energy dispersive spectroscopy. The microwave dielectric properties are measured at 6 GHz using a network analyzer. $Ba_5Nb_4O_{15}$ and/or $Ba_8(Co,Zn)_1Nb_6O_{24}$ secondary phases were found on the surface according to sintering conditions due to volatilization of some Zn and Co elements. The experimental results show that the beneficial effect of the annealing steps to improved the microwave dielectric properties. Excellent microwave dielectric properties were achieved for the coarse-grained microstructures by a higher sintering temperature and with a shorter holding time followed by annealing steps at lower temperatures with a longer holding time. This improvement can be attributed to 1:2 cation ordering within the crystal, which is taking place during annealing process. The $Ba(Co_{0.7}Zn_{0.3})_{1/3}Nb_{2/3}O_3$ ceramic could be used successfully for realization of dielectric microwave resonators, since it has a high quality factor Q_f value of 123,700 GHz, a high dielectric constant ε_r value of 34.5 and a temperature coefficient of the resonant frequency τ_f of 0 ppm/°C.

Keywords: ceramics; microstructure; X-ray diffraction; dielectric properties

1. Introduction

Compounds with perovskite structure with a general formula ABO_3 have been of continuous importance for many years [1]. The properties of perovskites depend critically on the nature of the metal atoms in the A and B sites. As a consequence, substitutions on the A and/or B sites allow varying their properties over wide ranges, which makes them adaptable to various technical requirements. Perovskites have numerous applications such as dielectric resonators, filters and antennas in a vast field of domains like wireless communication devices, radar, direct broadcasting satellites and global positioning systems [2–4]. Tantalum-based ceramics such as $Ba_3ZnTa_2O_9$ (BZT) and $Ba_3MgTa_2O_9$ (BMT) are frequently used as materials for dielectric resonators, despite the elevated tantalum price. As a consequence, a considerable amount of research is nowadays focused on the search for alternative ceramic materials providing comparable dielectric proprieties at lower

costs. Applications as dielectric resonators require materials with a high quality factor at the resonance frequency (Q_f), a high dielectric constant (ε_r) and a near-zero temperature coefficient of the resonance frequency (τ_f) [2,5]. In this context, $Ba(Co_{0.7}Zn_{0.3})_{1/3}Nb_{2/3}O_3$ (BCZN) ranks among the best oxide materials with regard to applications such as dielectric resonators in the range of microwave frequencies due to its high Q_f value (~56,000–85,000 GHz), its high ε_r (~34.5) and its small τ_f (~0) [6,7]. BCZN-based ceramics have therefore been suggested as a promising alternative to tantalum-based ceramics for applications in the microwave range. However, the dielectric properties of these ceramic materials are dependent on their density [8]. In addition, it is well known that BCZN-based ceramics are difficult to densify below 1450 °C [9]. In order to improve the sinterability of BCZN ceramics, we have successfully used the aqueous mixing technique-assisted solid-state method for the preparation of $Ba(Co_{0.7}Zn_{0.3})_{1/3}Nb_{2/3}O_3$ powders, which were sintered at 1350 °C for 30 h in air [10]. As a continuation of our previous work, the present paper describes improvements of the microwave dielectric proprieties of BCZN ceramics achieved by a supplementary annealing process, which is added to the synthesis procedure described previously. In this article, we study the effect of this additional annealing step on the structure, microstructure, and microwave dielectric properties of BCZN ceramics and compare the results with those obtained without this annealing. It will be shown that this second annealing step leads to a ~28% increase of the Q_f value. The improvement is explained by cation ordering within the crystal, as revealed by X-ray diffraction (XRD). The relationship between the heat treatment and the BCZN characteristics will be discussed in detail.

2. Experimental Section

The $Ba(Co_{0.7}Zn_{0.3})_{1/3}Nb_{2/3}O_3$ (BCZN) ceramics (LUSAC, Cherbourg, France) were prepared using the aqueous mixing technique-assisted solid-state method at 1000 °C for 2 h in air. The synthesis method is described in [10]. Pellets of a diameter of 10 mm and a thickness of 5 mm were formed by uniaxial (Carver, Wabash, IN, USA) pressing with 200 MPa. The ceramics were then sintered at two different temperatures and durations (1450 °C for 2 h and 1350 °C for 30 h). These samples are denoted hereafter as *S1* and *S2*, respectively. These sintered ceramics *S1* and *S2* were then submitted to an additional annealing step at 1300 °C for 30 h in air to study the effect of such an annealing on their structure and microstructure and on their microwave dielectric properties. Samples *S1* and *S2* having undergone this additional annealing procedure will be denoted hereafter as *S1a* and *S2a*, respectively. Thermodilatometric analysis was performed in air up to 1500 °C with a Seteram TMA92, using a heating/cooling rate of 150 °C·h^{-1}. The measurement was performed on cylindrical compacts having a height of 10 mm and a diameter of 5 mm, obtained by pressing the powders isostatically at 196 MPa. The sintered and annealed specimens were cooled inside the furnace under air atmosphere. All samples were heated and cooled at a rate of 200 °C·h^{-1}. X-ray diffraction was carried out at room temperature for the sintered and annealed samples by using a Inel Equinox 3000 diffractometer (Inel, Artenay, France) in air, employing CuK_α radiation (λ = 1.540562 Å) over the range of 2θ = 15–60°. A microstructural examination of the specimen was performed in a scanning electron microscope (SEM, Hitachi S3400, Tokyo, Japan) combined with an energy dispersive spectrometer (EDS, ThermoNoran Middleton, WI, USA). In addition, the experimental densities of the sintered pellets were measured on a Micromiretics accupyc 1330 helium pycnometer (Micromeritics, Norcross, GA, USA). Surfaces of the densified ceramics were polished successively using various grades of silicon carbide papers and 1.0 µm diamond paste was used for the final polishing. Afterwards the polished pellets were treated thermally at 1100 °C for 20 min. The purpose of this thermal etching consists in revealing the BCZN grain boundaries in a pre-polished sample by the formation of grooves in the intersections of BCZN grain boundaries. Finally, the dielectric properties were measured at 6 GHz resonance frequency using an Agilent 8722ES vector network analyzer (Agilent, Santa-Clara, CA, USA).

3. Results and Discussion

3.1. Thermodilatometry

Figure 1 shows the thermodilatometric measurements up to 1500 °C under air for calcined powders of BCZN ceramic materials. This experiment was performed in order to optimize the sintering temperature. As can be seen on the graph, shrinkage was observed to start at ~1090 °C. In addition, the derivative curve indicates a high densification rate (−1.7% min^{-1}) at 1350 °C and the maximum densification of BCZN is achieved at 1450 °C. Thus, two temperatures 1350 and 1450 °C, have been chosen to sinter the pellets with a heating and cooling rate of 200 °C· h^{-1} under air atmosphere. Regarding the durations, two sintering times were studied: 2 h and 30 h at 1350 °C and also at 1450 °C. It turned out that the best results are achieved by using a high temperature (1450 °C) during a short time (2 h) or by using a longer treatment (30 h) at a lower temperature (1350 °C). Taking into account these results and in order to study the effect of the heat treatment on the dielectric properties of the BCZN ceramics, we decided to describe here the sintering processes that provided the best dielectrics proprieties. Therefore, we chose to present the sintered pellets at 1350 °C for 30 h and at 1450 °C for 2 h under air atmosphere with a heating and cooling rate of 200 °C· h^{-1}.

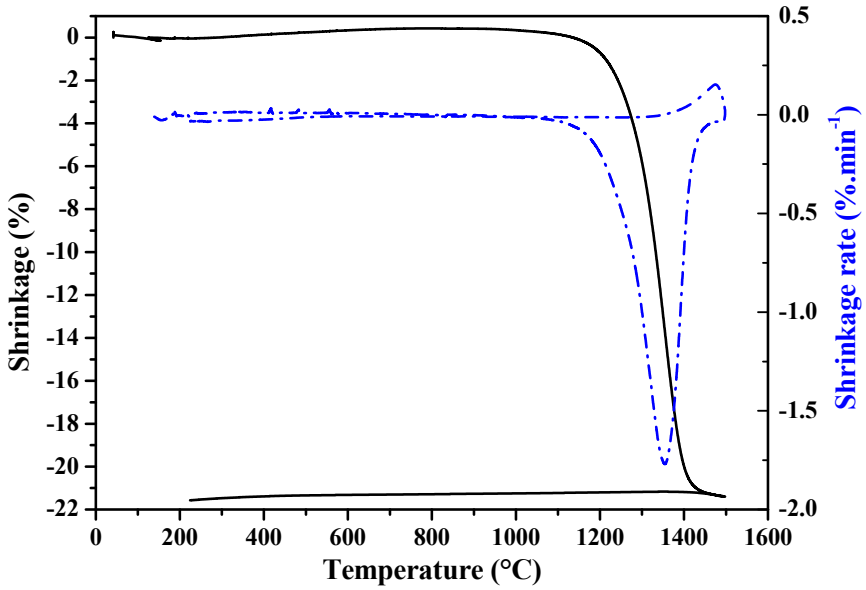

Figure 1. Shrinkage curve of a BCZN sample as a function of temperature.

3.2. Structural Characterization

Figures 2 and 3 show X-ray diffraction patterns of the $Ba(Co_{0.7}Zn_{0.3})_{1/3}Nb_{2/3}O_3$ (BCZN) ceramics after sintering at 1450 °C for 2 h (sample *S1*) and after annealing at 1300 °C (sample *S1a*) for 30 h. In order to identify the surface composition, the analyses were carried out at the upper surface for both specimens and at depths of 90 and 120 μm for sintered and annealed ceramics, respectively. It can be seen that the surface XRD pattern (Figure 2a) can be interpreted as a mixture of $Ba(Co_{0.7}Zn_{0.3})_{1/3}Nb_{2/3}O_3$ (BCZN) and $Ba_8(Co,Zn)_1Nb_6O_{24}$ phases. The complex perovskite ceramic $Ba_8(Co,Zn)_1Nb_6O_{24}$ is isostructural with $Ba_8Ni_1Nb_6O_{24}$ and $Ba_8Zn_1Nb_6O_{24}$ [11]. The Co:Zn ratio in $Ba_8(Co,Zn)_1Nb_6O_{24}$ may be variable.

At a depth of 90 μm below the surface (Figure 2b), all reflections can be attributed to the cubic structure of $Ba(Co_{0.7}Zn_{0.3})_{1/3}Nb_{2/3}O_3$, whereas no peaks attributable to $Ba_8(Co,Zn)_1Nb_6O_{24}$ were observed. These results clearly show that the $Ba_8(Co,Zn)_1Nb_6O_{24}$ phase is only formed on the surface of the BCZN ceramics and that it represents a secondary phase. The appearance of this phase is probably due to the volatilization of some Zn and Co elements during the sintering steps [12]. For

annealed ceramics (Figure 3), all diffraction peaks in Figure 3a (on the surface) can be attributed to the $Ba(Co_{0.7}Zn_{0.3})_{1/3}Nb_{2/3}O_3$ and $Ba_8(Co,Zn)_1Nb_6O_{24}$ phases. However, the relative intensities of the main peaks of the two phases are reversed as compared to those observed for the sintered materials, suggesting that the amount of $Ba_8(Co,Zn)_1Nb_6O_{24}$ increased on the surface of the BCZN ceramic after the annealing process. On the other hand, the patterns obtained at a depth of 120 microns below the surface (Figure 3b), are similar to those obtained at a depth of 90 μm after sintering (Figure 2b). The latter findings are consistent with previous works indicating that the core of the specimens consists only of the $Ba(Co_{0.7}Zn_{0.3})_{1/3}Nb_{2/3}O_3$ phase and that it transforms into $Ba_8(Co,Zn)_1Nb_6O_{24}$ at a high temperature on the surface [10]. The X-ray patterns also show a superlattice peak at 2θ = 17.74° (marked by an open circle), as shown in the small insert in Figure 3b. This reflection highlights the 1:2 cation ordering within the crystal [7]. The effect of the cation ordering on the dielectric proprieties of BCZN will be discussed in the following section in paragraph 3.4. The insert shows also the reflection peak at 2θ = 29.59° (marked by a sold star) arising from the $Ba_8(Co,Zn)_1Nb_6O_{24}$ phase. This indicates that the secondary phase of $Ba_8(Co,Zn)_1Nb_6O_{24}$ is located at a depths of over 120 μm.

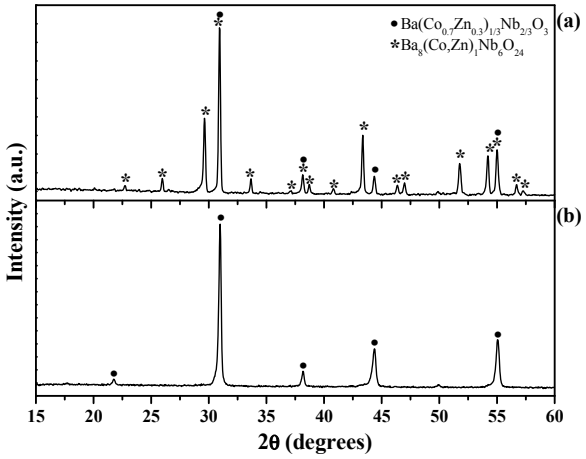

Figure 2. X-ray diffractograms of a BCZN ceramic (*S1*): (**a**) at the upper surface and (**b**) at a depth of 90 μm below the surface. •: $Ba(Co_{0.7}Zn_{0.3})_{1/3}Nb_{2/3}O_3$; *: $Ba_8(Co,Zn)_1Nb_6O_{24}$.

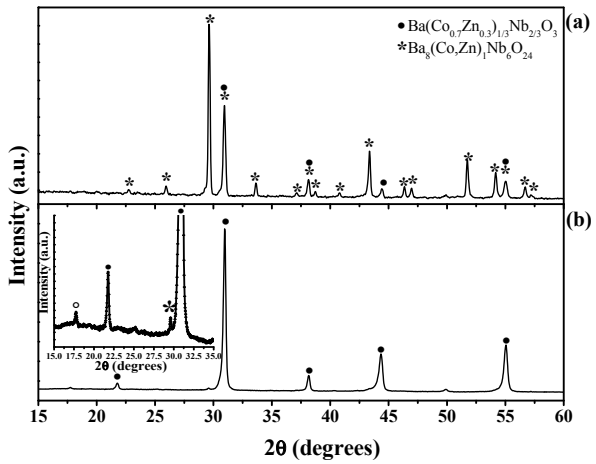

Figure 3. X-ray diffractograms of a BCZN ceramic (*S1a*): (**a**) at the upper surface and (**b**) at a depth of 120 μm below the surface. •: $Ba(Co_{0.7}Zn_{0.3})_{1/3}Nb_{2/3}O_3$; *: $Ba_8(Co,Zn)_1Nb_6O_{24}$. Inset: The region limited between 15° and 35° 2θ shows a superlattice peak for 1:2 ordering which is denoted by an open circle.

Figures 4 and 5 show X-ray diffraction patterns of the $Ba(Co_{0.7}Zn_{0.3})_{1/3}Nb_{2/3}O_3$ (BCZN) ceramics after sintering at 1350 °C for 30 h (sample *S2*) and after annealing at 1300 °C for 30 h (sample *S2a*). The analyses were carried out at the upper surface for both specimens and at depths of 120 and 140 μm for sintered and annealed ceramics, respectively. It can be seen that the surface XRD pattern (Figure 4a) can be interpreted as a mixture of three phases $Ba(Co_{0.7}Zn_{0.3})_{1/3}Nb_{2/3}O_3$ (BCZN), $Ba_5Nb_4O_{15}$ and $Ba_8(Co,Zn)_1Nb_6O_{24}$. At a depth of 120 μm below the surface (Figure 4b), all reflections can be attributed to the cubic structure of $Ba(Co_{0.7}Zn_{0.3})_{1/3}Nb_{2/3}O_3$ (BCZN), whereas no peaks attributable to $Ba_8(Co,Zn)_1Nb_6O_{24}$ or $Ba_5Nb_4O_{15}$ were observed. These results clearly show that the $Ba_8(Co,Zn)_1Nb_6O_{24}$ and $Ba_5Nb_4O_{15}$ phases are only formed on the surface of the BCZN ceramics and that they represent secondary phases. The origin of these phases is probably due to the volatilization of some Zn and Co elements during the sintering steps [12]. For post-sinter annealed ceramics it can be seen from Figure 5a that the XRD pattern confirms the presence of three phases on the surface of the ceramics: $Ba(Co_{0.7}Zn_{0.3})_{1/3}Nb_{2/3}O_3$ (BCZN), $Ba_5Nb_4O_{15}$ and $Ba_8(Co,Zn)_1Nb_6O_{24}$. In addition, the relative intensities of the $Ba_5Nb_4O_{15}$ and $Ba_8(Co,Zn)_1Nb_6O_{24}$ peaks increase, while those of the BCZN peaks decrease, suggesting that the amounts of the secondary phases of $Ba_8(Co,Zn)_1Nb_6O_{24}$ and $Ba_5Nb_4O_{15}$ increased on the surface of the BCZN ceramic after annealing. From the XRD pattern collected at the depth of 140 μm below the surface (Figure 5b), we can see that all peaks can be attributed to the $Ba(Co_{0.7}Zn_{0.3})_{1/3}Nb_{2/3}O_3$ phase. However, data analyses show some crystal diffraction peaks at $2\theta = 17.72°$ (marked by an open circle), which reflects the 1:2 cation ordering within the crystal already observed in previous work [7].

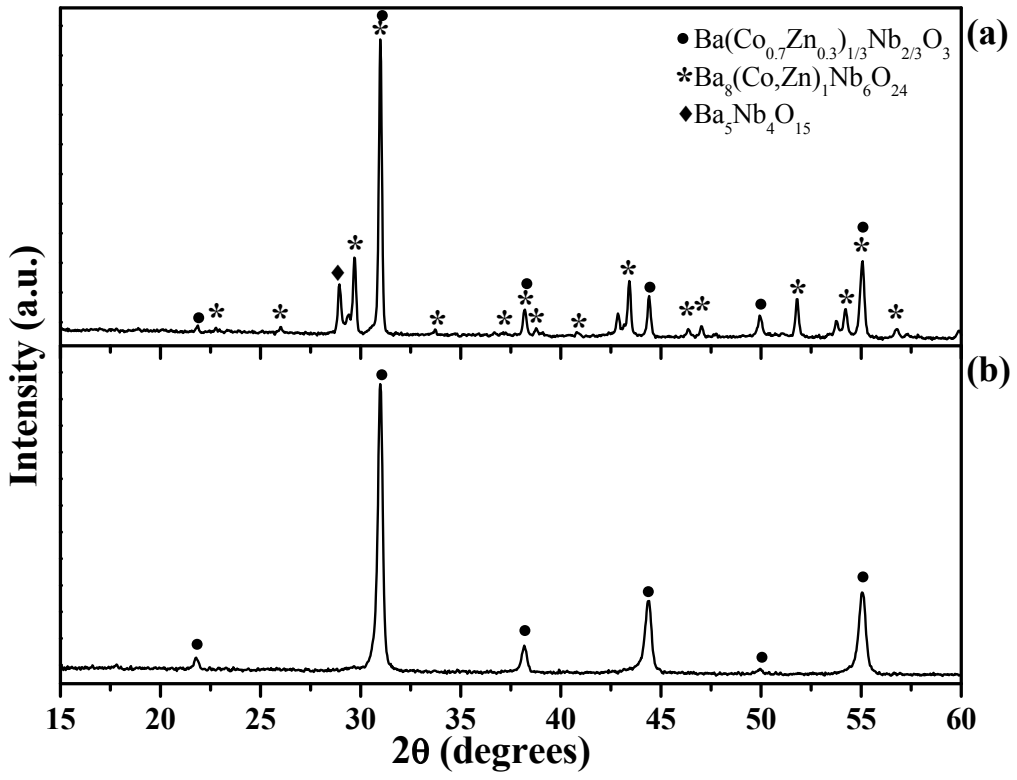

Figure 4. X-ray diffractograms of a BCZN ceramic (*S2*): (**a**) at the upper surface and (**b**) at a depth of 120 μm below the surface. •: $Ba(Co_{0.7}Zn_{0.3})_{1/3}Nb_{2/3}O_3$; *: $Ba_8(Co,Zn)_1Nb_6O_{24}$; ♦: $Ba_5Nb_4O_{15}$.

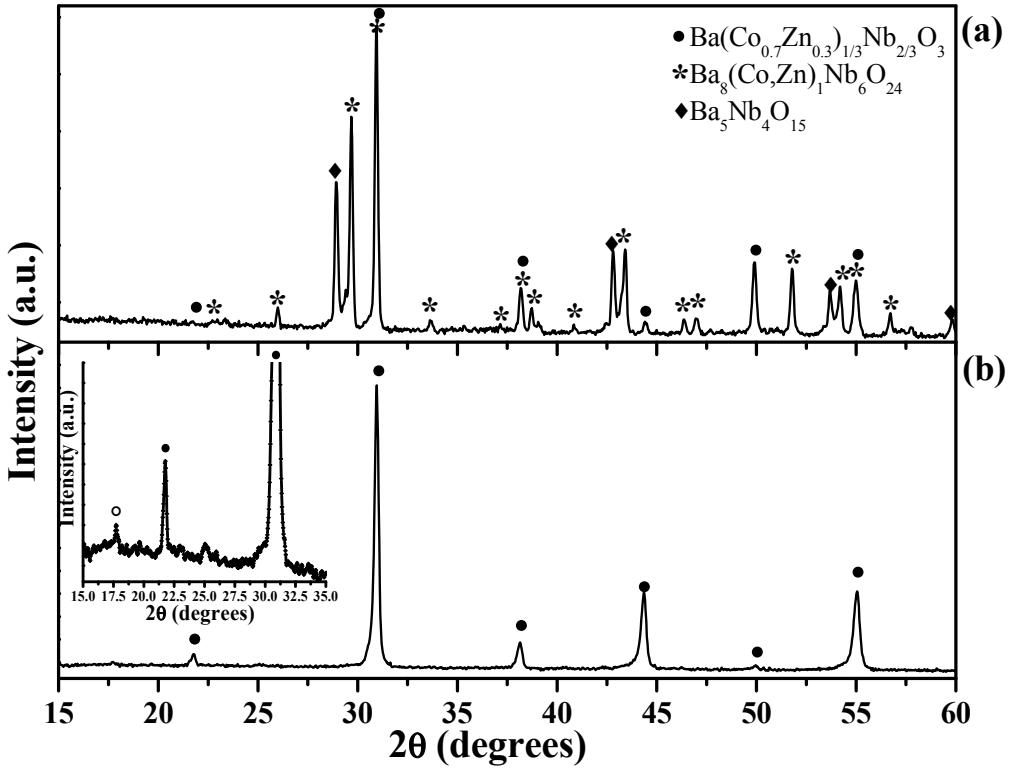

Figure 5. X-ray diffractograms of a BCZN ceramic (*S2a*): (**a**) at the upper surface and (**b**) at a depth of 140 µm below the surface. •: $Ba(Co_{0.7}Zn_{0.3})_{1/3}Nb_{2/3}O_3$; *: $Ba_8(Co,Zn)_1Nb_6O_{24}$; ♦: $Ba_5Nb_4O_{15}$. Inset: The region limited between 15° and 35° 2θ shows a superlattice peak for 1:2 ordering denoted by an open circle.

3.3. Microstructural Investigations

Figures 6 and 7 show SEM micrographs of the $Ba(Co_{0.7}Zn_{0.3})_{1/3}Nb_{2/3}O_3$ (BCZN) ceramics of samples *S1* and *S1a*, respectively. The SEM images were recorded (Figures 6a and 7a) on the surface; (Figures 6b and 7b) a fractured surface; (Figures 6c and 7c) on grain boundaries; (Figures 6d and 7d) and on longitudinally polished sections for these two cases just described. From Figure 6a it can be seen that the micrograph confirms the presence of two phases on the surface of the ceramics, needle-shaped grains and plate-shaped grains. Based on previous work, the needle-shaped grains are identified as $Ba_8(Co,Zn)_1Nb_6O_{24}$, while the plate-shaped grains consist of $Ba(Co_{0.7}Zn_{0.3})_{1/3}Nb_{2/3}O_3$ [10]. This result is in agreement with the XRD data (Figure 2a). The SEM image of the fractured surface (Figure 6b) reveals that the specimens consist of a single and homogeneous phase. Figure 6c shows a micrograph highlighting a grain boundary with a typical grain size of approximately 14 microns. In addition, the large amounts of residual pores were mainly located along the grain boundaries. This porosity is observed also in the fractured surface (Figure 6b) and in longitudinally polished sections (Figure 6d). Figure 6d is a backscattered SEM image of a longitudinally polished section of a BCZN ceramic. It can be seen that the surface clearly consists of two different domains, appearing as a light grey area (marked by 1) and a dark grey area (marked by 2) on the micrograph. In order to get a better insight into the chemical composition of these phases, EDS data were collected in these two areas.

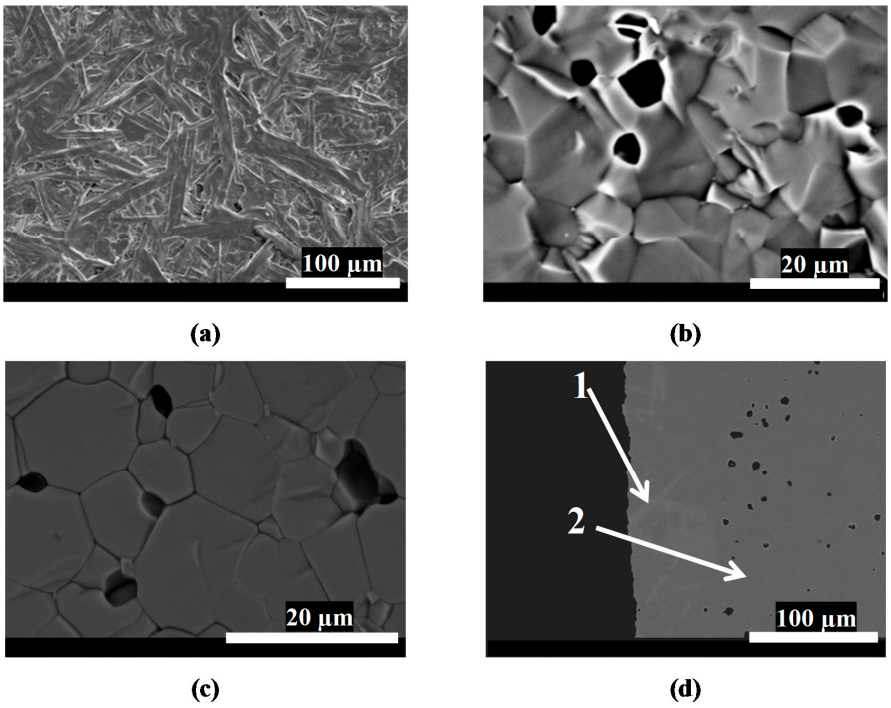

Figure 6. SEM micrographs of BCZN ceramics (*S1*): (**a**) of a surface; (**b**) of a fractured surface; (**c**) of a grain boundary; and (**d**) of a longitudinally polished section.

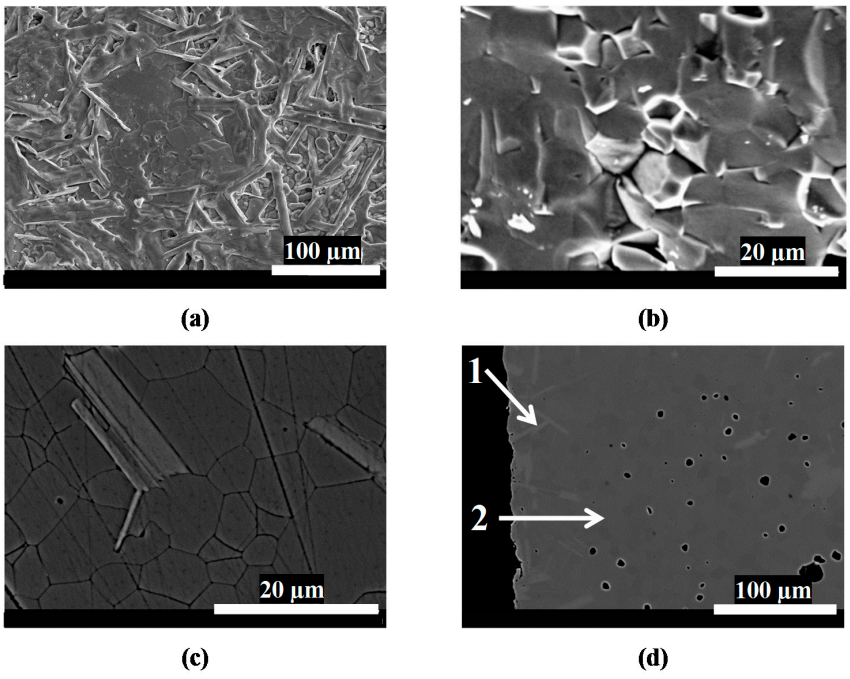

Figure 7. SEM micrographs of BCZN ceramics (*S1a*): (**a**) of a surface; (**b**) of a fractured surface; (**c**) of a grain boundary; and (**d**) of a longitudinally polished section.

The atomic percentages derived from the EDS spectra are given in Table 1. The atomic percentages of the light grey area (zone 1) are close to the theoretical values expected for $Ba_8(Co,Zn)_1Nb_6O_{24}$, while the percentages of the dark grey area (zone 2) agree quite well with those of $Ba(Co_{0.7}Zn_{0.3})_{1/3}Nb_{2/3}O_3$. Those two compounds were also identified by XRD at the surface of the specimen (Figure 2a).

Figure 7 shows the micrographs of the post-sinter annealed BCZN sample (*S1a*). The microstructure morphology observed after the annealing step was similar to that of the sintered sample (*S1*), while significant changes are identified in terms of density and surface composition of the specimen. Figure 7c reveals a persistent secondary phase in the surface of the specimens (needle-shaped grains). These results are also in agreement with the XRD analyses (Figure 3a). It is interesting to note that the annealing step at 1300 °C for 30 h has no effect on the grain growth. In contrast, secondary phase formation is very marked. The EDS analysis (Figure 7d), reveals a light grey area (zone 1) and a dark grey area (zone 2) comparable to the surface of the sintered ceramic (Figure 6d) as shown in Table 1.

Table 1. Atomic percentages obtained from EDS analyses on areas of interest by moving the analyzing spot. Zones 1 and 2 correspond to light grey and dark grey areas, respectively, mentioned in Figures 6d, 7d, 8d and 9d. These figures were performed on the samples *S1*, *S1a*, *S2* and *S2a*, respectively.

Investigated Area in the SEM Image		%O	%Ba	%Co	%Zn	%Nb	Attribution
Figure 6d (*S1*)	zone 1	61.3 ± 0.8 (*61.53*) *	19.5 ± 0.2 (*20.51*)	1.7 ± 0.2 (*1.86*)	0.62 ± 0.2 (*0.67*)	17.9 ± 0.2 (*15.38*)	$Ba_8(Co_{0.73}Zn_{0.27})_1Nb_6O_{24}$
	zone 2	59.6 ± 2.1 (*60*)	20.3 ± 0.2 (*20*)	4.9 ± 03 (*4.66*)	1.8 ± 0.3 (*2*)	13.3 ± 0.3 (*13.33*)	$Ba(Co_{0.7}Zn_{0.3})_{1/3}Nb_{2/3}O_3$
Figure 7d (*S1a*)	zone 1	59.1 ± 0.8	19.8 ± 0.2	1.6 ± 0.2	0.7 ± 0.2	18.6 ± 0.2	$Ba_8(Co_{0.73}Zn_{0.27})_1Nb_6O_{24}$
	zone 2	59.6 ± 1.4	19.1 ± 0.2	4.5 ± 0.2	1.9 ± 0.2	14.9 ± 0.2	$Ba(Co_{0.7}Zn_{0.3})_{1/3}Nb_{2/3}O_3$
Figure 8d (*S2*)	zone 1	62.1 ± 1.1	19.3 ± 0.2	1.7 ± 0.2	0.6 ± 0.1	16.2 ± 0.1	$Ba_8(Co_{0.73}Zn_{0.27})_1Nb_6O_{24}$
	zone 2	60.9 ± 1.0	18.9 ± 0.1	4.2 ± 0.1	1.4 ± 0.2	14.6 ± 0.1	$Ba(Co_{0.7}Zn_{0.3})_{1/3}Nb_{2/3}O_3$
Figure 9d (*S2a*)	zone 1	56.7 ± 0.7	19.5 ± 0.2	1.7 ± 0.2	0.49 ± 0.1	17.9 ± 0.1	$Ba_8(Co_{0.73}Zn_{0.27})_1Nb_6O_{24}$
	zone 2	59.8 ± 1.6	19.4 ± 0.2	4.4 ± 0.2	1.8 ± 0.2	14.6 ± 0.2	$Ba(Co_{0.7}Zn_{0.3})_{1/3}Nb_{2/3}O_3$

* Values in italics are those theoretically expected in the case of isolated particles. Deviations are in agreement with the presence of interfaces between phases detected by XRD. Zone 1: light grey area, zone 2: dark grey area.

Figures 8 and 9 show SEM micrographs of the BCZN ceramics after sintering and annealing steps. The SEM images were acquired under the same conditions as described above. Figure 8a–d shows the microstructures of sample *S2*. A significant change in microstructure was observed on these samples with a 0.6–2.3 μm fine grained microstructure developed at this sintering temperature, with very few residual pores mainly located along grain boundaries (Figure 8c).

Figure 9a–d shows the microstructures of the post-sinter annealed BCZN sample (*S2a*). No significant difference is found in the microstructure after the annealing process. However, increasing grain sizes were observed with increasing annealing time at 1300 °C, with a typical grain size of 0.9–4 micron (Figure 9c). These results demonstrate that the sintering condition has a significant effect on the structure and microstructure of the BCZN specimen. The grain size increases at sintering temperatures above 1300 °C, whereas the secondary phase remains on the specimen surface even after sintering for a longer time.

The results obtained by EDS analysis (Figures 8 and 9) for the light grey area (zone 1) and the dark grey area (zone 2) are also given in Table 1. The light grey area consists essentially of $Ba_8(Co,Zn)_1Nb_6O_{24}$ and the dark grey area of $Ba(Co_{0.7}Zn_{0.3})_{1/3}Nb_{2/3}O_3$. Those two compounds were also identified by XRD (Figures 4a and 5a). However, we note the absence of the characteristic signal of $Ba_5Nb_4O_{15}$. This can be explained by a fine layer of $Ba_5Nb_4O_{15}$, located on the upper surface, while $Ba_8(Co,Zn)_1Nb_6O_{24}$ is located below the surface. Thus, according to the sintering condition, the surface of the BCZN ceramics consists in a mixture of two or three phases. $Ba(Co_{0.7}Zn_{0.3})_{1/3}Nb_{2/3}O_3$, $Ba_8(Co,Zn)_1Nb_6O_{24}$ and $Ba_5Nb_4O_{15}$ for the specimen (*S1*) sintered at 1450 °C for 2 h and only $Ba(Co_{0.7}Zn_{0.3})_{1/3}Nb_{2/3}O_3$ and $Ba_8(Co,Zn)_1Nb_6O_{24}$ for the specimen (*S2*) sintered at 1350 °C for 30 h. In contrast, the core of the specimens is only composed of the $Ba(Co_{0.7}Zn_{0.3})_{1/3}Nb_{2/3}O_3$ matrix, whatever the sintering and annealing conditions were. The black spots observed in the SEM image (Figures 8d and 9d) represent a residual porosity.

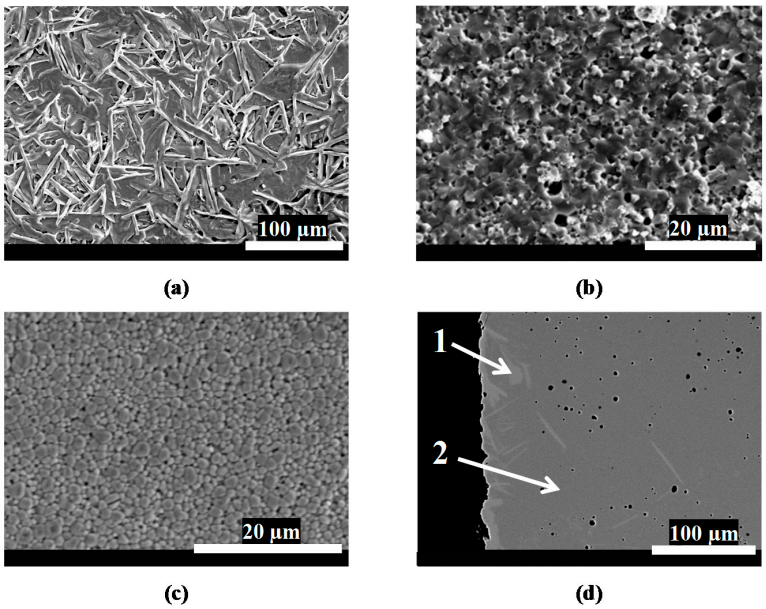

Figure 8. SEM micrographs of BCZN ceramics (*S2*): (**a**) of a surface; (**b**) of a fractured surface; (**c**) of a grain boundary; and (**d**) of a longitudinally polished section.

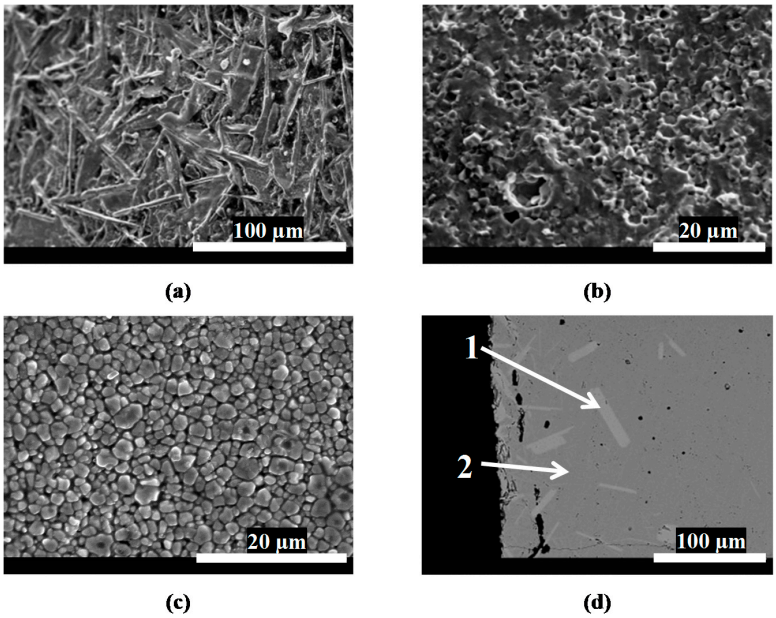

Figure 9. SEM micrographs of BCZN ceramics (*S2a*): (**a**) of a surface; (**b**) of a fractured surface; (**c**) of a grain boundary; and (**d**) of a longitudinally polished section.

3.4. Microwave Dielectric Properties

The microwave dielectric properties of the $Ba(Co_{0.7}Zn_{0.3})_{1/3}Nb_{2/3}O_3$ ceramics were investigated for specimens *S1*, *S2*, *S1a* and *S2a*. The measurements were recorded from polished and unpolished samples. No significant differences in dielectric properties were observed before and after polishing. This is due to their good microwave dielectric properties [9]. This observation suggests that the secondary phases of $Ba_8(Co,Zn)_1Nb_6O_{24}$ and of $Ba_5Nb_4O_{15}$ seem to have no effect on the dielectric properties. The results of the dielectric measurements at about 6 GHz are gathered in Table 2.

As displayed in Table 2, the sintering and annealing steps seem to have little effect on the dielectric constant εr and on the temperature coefficient of the resonant frequency τ_f, whereas the

quality factor Q_f at 6 GHz is significantly affected. Thus, a high quality factor Q_f of 96,132 GHz, a high dielectric constant εr of 34.5 and a temperature coefficient of the resonant frequency τ_f of 0 ppm/°C were obtained for sample *S2* (Table 2). The relative density of this specimen (*S2*) is about 6.29 indicating a high density of the obtained ceramic materials. On the other hand, a similar quality factor Q_f of 99,700 GHz is obtained for the annealed sample *S2a* (Table 2) with a relative density of 6.55. In the case of specimen *S1* (Table 2), a Q_f value of 36,953 GHz is observed with a relative density of 6.44. The latter value of Q_f is much lower than that obtained for specimen *S2*. However, the Q_f value of the ceramics were remarkably improved by the annealing process at 1300 °C for 30 h and the maximum Q_f value of BCZN sample (*S1a*) was 123,700 GHz, which is 25% higher than that of BCZN sample (*S1*) (Table 2). The relative density of the latter specimen is 6.56 (~96% of the theoretical density). The results in Table 2 show that high densities were obtained for all ceramics materials regardless of the processing conditions. This confirms that, from certain density values on (>90%), the Q_f value is independent of the density in agreement with previous data [13]. Indeed, during the sintering step, the improved Q_f value could be linked to differences in the ceramic microstructure as shown in Table 2, with a high Q_f value of 96132 was obtained for the BCZN specimen (*S2*), with a grain size of 0.6–2.3 microns. During the annealing process, the quality factor Q_f of the BCZN ceramics was significantly improved. It can be seen from Table 2, that the high values of Q_f of 99,700 and 123,700 GHz are observed of the annealed samples *S2a* and *S1a*, respectively. This improvement of the Q_f-value is explained by 1:2 cation ordering in accordance with the XRD data recorded on the surface of the post-sinter annealed ceramics (*S1a* and *S2a*), as shown in the small insert figure in Figures 3b and 5b, respectively. A similar result was previously reported which shows the increase of the Q_f values as a consequence of cation ordering [9]. This Q_f value of 123,700 GHz is higher than those obtained for the undoped and Al_2O_3-doped BCZN ceramics (Q_f = 115,307 and 61,056 GHz, respectively), published recently [14,15], indicating that the $Ba(Co_{0.7}Zn_{0.3})_{1/3}Nb_{2/3}O_3$ materials are promising candidates for microwave device applications.

Table 2. Characteristics and dielectric properties (measured at 6 GHz) of BCZN specimens *S1*, *S2*, *S1a* and *S2a*.

Heat Treatment Conditions and Sample Name		Density (g/cm^3)	ε_r	τ_f (ppm/°C)	Q_f (GHz)	Order	Grain Size (μm)
Sintering process	(*S2*):1350 °C for 30 h	6.29	~34.5	~0	96,132	–	0.6–2.3
	(*S1*):1450 °C for 2 h	6.44	~34.5	~0	36,953	–	~14
Annealing process	(*S2a*):1300 °C for 30 h	6.56	~34.5	~0	99,700	+	0.9–4
	(*S1a*):1300 °C for 30 h	6.47	~34.5	~0	123,700	+	~14

a Italic letter corresponds to annealing process of the BCZN ceramics. (−,+) Absence, Presence of the characteristic signal of 1:2 cation ordering within the crystal.

4. Conclusions

Densified ceramics with a BCZN Perovskite-type structure were prepared by a simple method using the aqueous mixing technique-assisted solid-state method. X-ray diffraction shows that $Ba_5Nb_4O_{15}$ and/or $Ba_8(Co,Zn)_1Nb_6O_{24}$ were found as secondary phases on the surface, depending on the sintering conditions. This study demonstrated that a higher sintering temperature with a shorter holding time followed by annealing steps at lower temperatures with a longer holding time are very important to produce microwave dielectric materials. Excellent microwave dielectric properties were achieved for the coarse-grained microstructures after sintering and annealing steps at 1450 °C for 2 h and at 1300 °C for 30 h, respectively. These process conditions represent the optimal sintering and annealing conditions to produced $Ba(Co_{0.7}Zn_{0.3})_{1/3}Nb_{2/3}O_3$ microwave dielectric materials. BCZN ceramics (*S1a*) prepared under these conditions exhibit a high quality factor Q_f of 123,700 GHz measured at 6 GHz, a high dielectric constant ε_r of 34.5 and a temperature

coefficient of the resonant frequency τ_f of 0 ppm/°C. All the characteristics of the prepared $Ba(Co_{0.7}Zn_{0.3})_{1/3}Nb_{2/3}O_3$ suggest its suitability for applications in the microwave range.

Acknowledgments: The authors gratefully acknowledge support from the French ANR under Contract No. ANR-08-MAPR-0013 project "Cheapcomponents". We wish to thank our industrial partner: TEMEX Ceramics.

Author Contributions: All the authors have made significant contributions to this study and have approved this submission. Brahim Itaalit and Mohamed Mouyane prepared the powders and the ceramics materials. Mohamed Mouyane, Brahim Itaalit, David Houivet and Jérôme Bernard carried out the experiments. Mohamed Mouyane, Jerôme Bernard, Manfred Womes and David Houivet contributed to analysis and interpretation of data. Mohamed Mouyane and Manfred Womes prepared the manuscript.

Conflicts of Interest: The authors declare no conflict of interest.

References

1. Luck, F. Wet air oxidation: Past, present and future. *Catal. Today* **1999**, *53*, 81–91. [CrossRef]
2. Chen, Y.C. Microwave dielectric properties of $(Mg_{(1-x)}Co_x)_2SnO_4$ ceramics for application in dual-band inverted-E-shaped monopole antenna. *IEEE Trans. Ultrason. Ferroelectr. Freq. Control* **2011**, *58*, 2531–2538. [CrossRef] [PubMed]
3. Sebastian, M.T. *Dielectric Materials for Wireless Communication*; Elsevier: Amsterdam, the Netherland, 2008.
4. Wersing, W. Microwave ceramics for resonators and filters. *Curr. Opin. Solid State Mater. Sci.* **1996**, *1*, 715–731. [CrossRef]
5. Scott, R.I.; Thomas, M.; Hampson, C. Development of low cost, high performance $Ba(Zn_{1/3}Nb_{2/3}O_3)$ based materials for microwave resonator applications. *J. Eur. Ceram. Soc.* **2003**, *23*, 2467–2471. [CrossRef]
6. Endo, K.; Fujimoto, K.; Murakawa, K. Dielectric properties of ceramics in $Ba(Co_{1/3}Nb_{2/3})O_3$-$Ba(Zn_{1/3}Nb_{2/3})O_3$ solid solutions. *J. Am. Ceram. Soc.* **1987**, *70*, 215–218. [CrossRef]
7. Ahn, C.-W.; Jang, H.-J.; Nahm, S.; Park, H.-M.; Lee, H.-J. Effect of microstructure on the microwave dielectric properties of $Ba(Co_{1/3}Nb_{2/3})O_3$ and (1-x)$Ba(Co_{1/3}Nb_{2/3})O_{3-x}Ba(Zn_{1/3}Nb_{2/3})O_3$ solid solutions. *J. Eur. Ceram. Soc.* **2003**, *23*, 2473–2478. [CrossRef]
8. Huang, C.-L.; Chien, Y.-H.; Shih, C.-F.; Chang, H.-Y. Crystal structure and dielectric properties of xCa$(Mg_{1/3}Nb_{2/3})O_3$-$(1-x)(Ca_{0.61}Nd_{0.26})TiO_3$ at the microwave frequency. *Mater. Res. Bull.* **2015**, *63*, 1–5. [CrossRef]
9. Azough, F.; Leach, C.; Freer, R. Effect of CeO_2 on the sintering behaviour, cation order and properties of $Ba_3Co_{0.7}Zn_{0.3}Nb_2O_9$ ceramics. *J. Eur. Ceram. Soc.* **2006**, *26*, 1883–1887. [CrossRef]
10. Abakumov, A.M.; Tendeloo, G.V.; Scheglov, A.A.; Shpanchenko, R.V.; Antipov, E.V. The crystal structure of $Ba_8Ni_1Nb_6O_{24}$: Cation ordering in hexagonal perovskites. *J. Solid State Chem.* **1966**, *125*, 102–107. [CrossRef]
11. Itaalit, B.; Mouyane, M.; Bernard, J.; Reboul, J.-M.; Houivet, D. Improvement of microwave dielectric properties of $Ba(Co_{0.7}Zn_{0.3})_{1/3}Nb_{2/3}O_3$ ceramics prepared by solid-state reaction. *Ceram. Int.* **2015**, *41*, 1937–1942. [CrossRef]
12. Azough, F.; Leach, C.; Freer, R. Effect of nonstoichiometry on the structure and microwave dielectric properties of $Ba(Co_{1/3}Nb_{2/3})O_3$ ceramics. *J. Eur. Ceram. Soc.* **2006**, *26*, 2877–2884. [CrossRef]
13. Kim, W.S.; Kim, T.H.; Kim, E.S.; Yoon, K.H. Microwave dielectric properties and far infrared reflectivity spectra of the $(Zr_{0.8}Sn_{0.2})TiO_4$ ceramics with additives. *Jpn. J. Appl. Phys.* **1998**, *37*, 5367–5371. [CrossRef]
14. Wang, Z.F.; Huang, B.Y.; Wang, L.X.; Fu, Z.X.; Zhang, Q.T. Effects of MnO_2 addition on quality factor of $Ba(Co_{0.7}Zn_{0.3})_{1/3}Nb_{2/3}O_3$ microwave dielectric ceramics. *Mater. Lett.* **2015**, *141*, 272–274. [CrossRef]
15. Liao, P.; Qiu, T.; Yang, J.; Lu, X. Effect of Al_2O_3 addition on microwave dielectric properties of $BaCo_{0.194}Zn_{0.116}Nb_{0.69}O_3$ ceramics. *Electron. Mater. Lett.* **2014**, *10*, 121–125. [CrossRef]